Reducing depth induced spherical aberration in 3D widefield fluorescence microscopy by wavefront coding using the SQUBIC phase mask

Nurmohammed Patwary[1], Ana Doblas[2], Sharon V. King[1], and Chrysanthe Preza[1♦],
[1]Dept. of Electrical and Computer Engineering, The Univ. of Memphis, Memphis, TN, USA
[2]Dept. of Optics, Univ. of Valencia, E-46100, Burjassot, Spain

ABSTRACT

Imaging thick biological samples introduces spherical aberration (SA) due to refractive index (RI) mismatch between specimen and imaging lens immersion medium. SA increases with the increase of either depth or RI mismatch. Therefore, it is difficult to find a static compensator for SA[1]. Different wavefront coding methods[2,3] have been studied to find an optimal way of static wavefront correction to reduce depth-induced SA. Inspired by a recent design of a radially symmetric squared cubic (SQUBIC) phase mask that was tested for scanning confocal microscopy[1] we have modified the pupil using the SQUBIC mask to engineer the point spread function (PSF) of a wide field fluorescence microscope. In this study, simulated images of a thick test object were generated using a wavefront encoded engineered PSF (WFE-PSF) and were restored using space-invariant (SI) and depth-variant (DV) expectation maximization (EM) algorithms implemented in the COSMOS software[4]. Quantitative comparisons between restorations obtained with both the conventional and WFE PSFs are presented. Simulations show that, in the presence of SA, the use of the SIEM algorithm and a single SQUBIC encoded WFE-PSF can yield adequate image restoration. In addition, in the presence of a large amount of SA, it is possible to get adequate results using the DVEM with fewer DV-PSFs than would typically be required for processing images acquired with a clear circular aperture (CCA) PSF. This result implies that modification of a widefield system with the SQUBIC mask renders the system less sensitive to depth-induced SA and suitable for imaging samples at larger optical depths.

Keywords: Three-dimensional microscopy, wavefront encoding, point-spread function engineering, image restoration, phase mask.

1. INTRODUCTION

The wavefront encoding technique has been implemented successfully in point-spread function (PSF) engineering[3] by placing a phase mask at the back focal plane of the microscope objective. The PSF is aberrated due to the refractive index (RI) mismatch between the immersion medium of the microscope objective lens and the object mounting medium. Spherical aberration (SA) increases with increased focal depth and due to this depth dependence, spherical aberration is a dynamic process. Spherical aberration reduces image resolution and increases the complexity of computational optical sectioning microscopy (COSM). Different depth variant restoration methods have been developed to address the depth variability of the PSF that add computational burden. To address this problem we test a wavefront modification designed to decrease the depth dependency of PSFs. Pupil modification by a phase mask has been studied in extended depth-of-field (EDOF) microscopy[3] where a cubic phase mask (CPM) was designed to gain EDOF. In EDOF imaging an intermediate encoded image is taken using a modified pupil and a computational process decodes this image. EDOF with a generalized cubic phase mask (GCPM) has been successfully studied in 3D computational microscopy[2]. In addition, adaptive optics and depth-variant deconvolution algorithms[6] have also been used to counteract spherical aberration[7-9]. A strata based model in the restoration process[5] represents the volume using multiple PSFs computed at specific depths to mitigate the depth variability of the PSFs. Performance of this approach depends on the thickness of the object. The number of PSFs required increases with the increase of thickness and so does the computational burden and memory requirement. Principal component analysis (PCA) is another approach to solve the depth-variant imaging problem[10, 11]

♦cpreza@memphis.edu; phone 1 901 678-4369; fax 1 901 678-5469; cirl.memphis.edu

Three-Dimensional and Multidimensional Microscopy: Image Acquisition and Processing XXI,
edited by Thomas G. Brown, Carol J. Cogswell, Tony Wilson, Proc. of SPIE Vol. 8949, 894911
 · doi: 10.1117/12.2040191

which minimizes the computational burden in restoration process but at the same time requires a lot of memory for an accurate PCA component calculation. These approaches work well in that they produce results in which artifacts due to SA are minimized, but they require a high performance computation facility. Hence, a simpler solution would be to reduce the PSF depth variability of the PSFs.

Recently, a simple but effective phase mask (SQUBIC) has been reported[1] to reduce the SA impact over a large range of depth. This phase mask works effectively in reducing wavefront distortion, and hence makes the PSF invariable over a large range of depth. This depth invariability makes object restoration from the blurred image using a single PSF over a wide range feasible. In this paper, we show the performance of the SQUBIC phase mask in 3D fluorescence microscopy in restoring a 3D object. Both qualitative and quantitative comparison is presented to show the improvement gained by using SQUBIC phase mask in the back focal plane in lieu of the conventional CCA system. This paper is organized as follows. Section 2 describes the background and theory behind SQUBIC WFE-PSF. Section 3 and 4 include the simulation methods and results, respectively. Summary of conclusions and future possible improvements are discussed in Section 5.

2. BACKGROUND

2.1 SQUBIC encoded WFE-PSF

Depth induced spherical aberration comes from the wavefront distortion due to the propagation of light within layers with RI mismatch, which depends on light wavelength, object RI, and numerical aperture (NA) of the objective lens. All these factors introduce different degrees of freedom and make SA a dynamic process. The idea of the SQUBIC phase mask is to apply a fixed dominant wavefront distortion via a phase mask $\phi = 2\pi A\varphi(\rho,\alpha)$ [1] at the back focal plane of the objective lens. To address different imaging conditions and design parameters, variation of the value of A is considered in order to vary the amount of wavefront distortion applied. Efficiency of the SQUBIC phase mask increases with the increase of A. In practice, the microscope objective's back focal plane is projected on a spatial light modulator (SLM) through a 4F optical system and the SLM resolution limits the value of A[16]. The phase function $\varphi(\rho,\alpha)$ is defined as[1] :

$$\varphi(\rho,\alpha) = \left[\frac{\sqrt{1-\rho^2\sin^2(\alpha)}-1}{1-\cos(\alpha)}+\frac{1}{2}\right]^3 \tag{1}$$

where ρ is a normalized pupil radius, $\alpha = \sin^{-1}\left(NA/n\right)$ and n is the refractive index of the lens' immersion medium.

2.2 3D DV WFE-PSF formation

In optical sectioning microscopy, a 3D volume is acquired by optically slicing the sample through the axis of light propagation (Z-axis) and capturing 2D images at multiple depths. When the specimen emitted wavefront passes through the objective lens, its Fourier transform is generated at the back focal plane[12] . To calculate WFE-PSFs from CCA PSFs, a generalized pupil function is calculated by taking the Fourier transform of the CCA PSF slices and adding the SQUBIC phase function $\phi(f_x, f_y)$ to the CCA pupil phase of each slice. This process is described by[2] :

$$h_{z_i,z_o}(x,y) = \left|F^{-1}\left\{H(f_x,f_y)e^{j(2\pi/\lambda)W(f_x,f_y;z_i,z_o)}e^{j\phi(f_x,f_y)}\right\}\right|^2 \tag{2}$$

where, $F^{-1}\{\bullet\}$ is 2-D inverse Fourier transform, $H(f_x,f_y)$ is clear circular aperture pupil function , λ is the emission wavelength, and $W(f_x,f_y;z_i,z_o)$ is the optical path length error due to defocus and SA as a function of the normalized spatial frequencies f_x and f_y .

2.3 Forward model formation

The forward image is simulated by computing 3D DV-PSFs at each layer using the superposition integral[2] :

$$g(\mathbf{x_i}) = \iiint_O h_{WFE}(x_i - x_o, y_i - y_o, z_i, z_o) s(\mathbf{x}_o) d\mathbf{x_0} \tag{3}$$

where, $\mathbf{x_i} = (x_i, y_i, z_i)$ is a point in the image space, $\mathbf{x}_o = (x_o, y_o, z_o)$ is a point in the object space ***O*** and $s(\mathbf{x_o})$ is the object of interest.

2.4 Image restoration

Intermediate images, simulated using the forward model, are restored using the space invariant expectation maximization (SIEM)[13] and the depth variant expectation maximization (DVEM)[5] algorithms. Both methods are iterative. In SIEM process, only one single PSF is used to restore the whole volume where in the DVEM method multiple DV-PSFs are used to restore the total volume. In the restoration process the region of interest (ROI) is divided in the axial direction into multiple strata and a PSF is computed at the edge of each stratum. Hence, the number of PSFs required in DVEM is equal to the number of strata plus one. The number of 3D deblurring computations needed is equal to the number of strata. As 3D deblurring is a computationally costly process, complexity increases with the increase in number of strata. A higher number of strata is required to achieve a more accurate restoration result. Both these algorithms are implemented in *CosmEstimation* module COSMOS[4] .

3. SIMULATION METHODS

3.1 Depth-variant (DV) PSF

Two hundred CCA DV-PSFs were calculated in MATLAB using the Gibson-Lanni optical path distance (OPD) model[14] and vectorial field approximation[15] at an interval of 0.3 µm to cover 60 µm depth. PSFs were calculated on a 128×128×1024 grid with a voxel size 0.1 µm × 0.1 µm × 0.1 µm with the following parameters: (a) the light point source is located at varying depth (starting from 0 µm to 60 µm with 0.3 µm spacing) in water (RI, $n_{water\,=}$ 1.33) below the coverslip (b) a 20X/0.8 NA objective lens and (c) the emission wavelength $\lambda_{emmision}$ = 515 µm. The voxel size is chosen to satisfy the Nyquist criteria. To compute WFE-PSFs, CCA PSF data were oversampled and over-ranged i.e., the number of pixels in the x-y plane was increased by the oversampling factor (we note that if over-ranging and oversampling is done by the same factor, the frequency domain sampling remains the same). WFE-PSFs were calculated from the CCA PSFs using the methods described in section 2.2. We used *A* = 88 to compute the SQUBIC phase mask.

3.2 Test object and forward image formation

To demonstrate the performance of the engineered PSF with the SQUBIC phase mask, three different types of object were studied. Test object 1 (Fig. 3a) consists of three small spheres (3 µm in diameter). Coordinates of the bead centers are (16.8 µm, 12.5 µm, 20 µm), (16.8 µm, 16.8 µm, 30 µm), (16.8 µm, 21.1 µm, 40 µm) respectively. The RI of the mounting medium is assumed to be 1.33, while the immersion medium of the lens is air (i.e., RI = 1.00). A second synthetic object (Fig. 3e) has only one 3-µm in diameter bead and depth position of that bead was varied from 20 µm to 40 µm. Test object 3 has five spherical beads of 3-µm diameter (Fig. 2a). The beads are centered at different (*x,y,z*) coordinates: (16.8 µm, 8.3 µm, 10 µm), (16.8 µm, 12.5 µm, 20 µm), (16.8 µm, 16.8 µm, 30 µm), (16.8 µm, 21.1 µm, 40 µm) and (16.8 µm, 25.3 µm, 50 µm) respectively. All synthetic objects are simulated on a 336×336×600 grid where each voxel size is 0.1 µm × 0.1 µm × 0.1 µm. The object is set within a larger grid (336×336×1250) to allow enough empty space to completely capture the intensity of the blurred images. A 7×7×7 Gaussian kernel with standard deviation 2.5 is used to smooth the object. This test object is convolved with all 200 PSFs using the *variant* tab of the *CosmTools*[4] to compute the simulated image, referred to here as the forward model image, (see Fig. 2b & c) and restored using *CosmEstimation* module of COSMOS software.

4. RESULTS AND DISCUSSION

4.1 WFE-PSFs using SQUBIC phase mask:

Fig. 1 shows CCA and SQUBIC WFE PSFs at different depths below the coverslip. Fig. 1a and Fig. 1b show the XZ view of CCA PSF at 0 µm and at 50 µm respectively. Two large differences between these two PSFs are observed. First, the CCA PSF location shifts along the axial direction. Second, the CCA PSF at 0 µm is symmetric along z- axis, but with the PSF at increased depth is asymmetric and extends along z-axis. Fig. 1e shows the XZ profile of the CCA PSFs along the maximum intensity point. Fig. 1c and Fig. 1d show XZ views of SQUBIC WFE-PSFs at 0 µm and at 50 µm, respectively and Fig. 1f shows the corresponding XZ profiles. From the XZ view of the SQUBIC WFE-PSFs it is qualitatively seen that the PSF only shifts along the axial direction without changing its shape at increased depth. To further quantify the WFE-PSF's variability compared to the PSF of the CCA system, the 3D normalized mean square error (NMSE) was calculated:

$$NMSE_{3D} = \frac{\left\langle \left\| h_0(x,y,z) - h_i(x,y,z) \right\| \right\rangle^2}{\left\langle \left\| h_0(x,y,z) \right\| \right\rangle^2} \qquad (4)$$

where, $h_0(x,y,z)$ is the PSF at zero depth and $h_i(x,y,z)$ is the PSF at some other depth. To compute the $NMSE_{3D}$, the axial shift of the PSF is compensated by registering the maximum intensity planes between the PSFs used in the computation. Fig. 1g shows the $NMSE_{3D}$ vs depth curve. It is seen that, the $NMSE_{3D}$ increases more rapidly in the case of CCA imaging compared to SQUBIC WFE imaging which infers the reduced depth sensitivity of the modified imaging system.

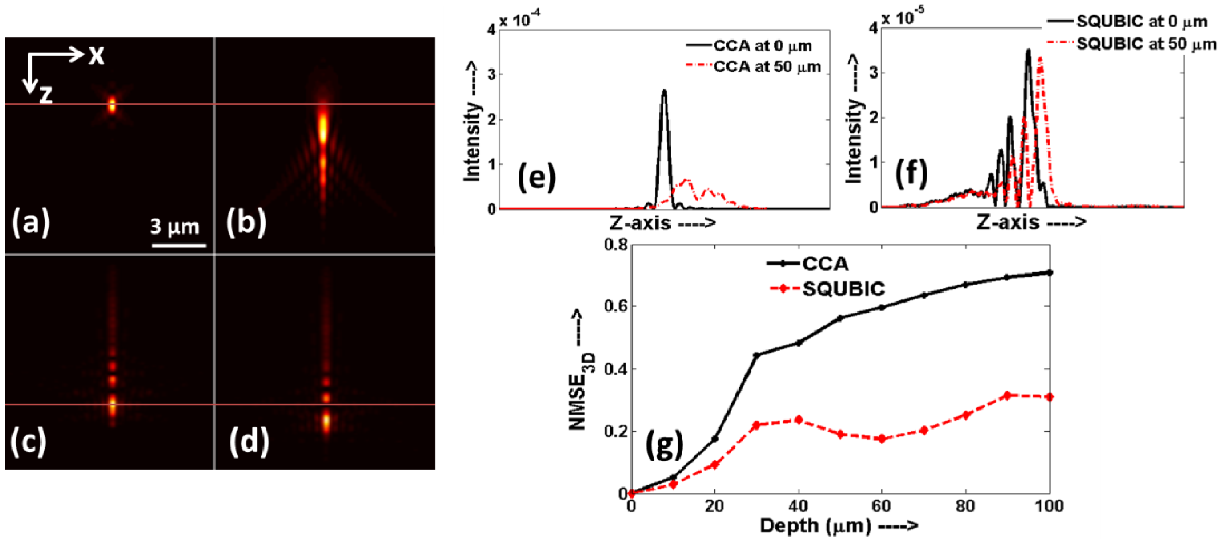

Fig. 1: PSF engineering with SQUBIC phase mask. (a) CCA-PSF at 0 µm, (b) CCA-PSF at 50 µm, (c) SQUBIC-PSF at 0 µm, (d) SQUBIC-PSF at 50 µm, (e) axial profile though the center of CCA-PSFs computed at 0 µm and 50 µm, (f) axial profile through the center of SQUBIC-PSFs computed at 0 µm and 50 µm, (g) normalized mean square error between PSF computed at 0 µm and other PSFs computed at different location. Lens used: 20x/0.8 NA air wavelength 515 nm.

4.2 Forward image

Simulated images of a test object demonstrate that SQUBIC WFE imaging suffers less variability due to depth-induced spherical aberration. Simulated forward images were computed using the method described is section 3.2. Fig. 2a shows the object with five similar spherical beads (object 3 as described in section 3.2). Fig. 2b is the simulated forward image in case of CCA imaging system and Fig. 2c is the corresponding simulated forward images in case of SQUBIC WFE imaging. Although the image of each bead appears more distorted in the SQUBIC image than the CCA image, it is invariant to depth in contrast to the CCA image in which images of beads at deeper depth show more axial asymmetry.

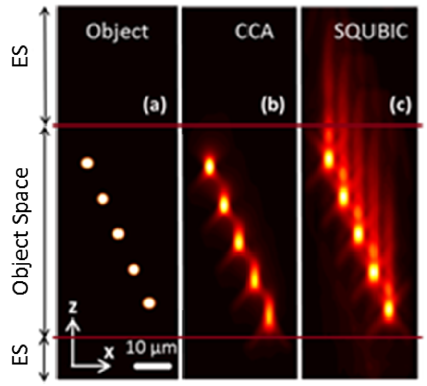

Fig. 2: Simulated forward CCA image and SQUBIC intermediate images. (a) A synthetic 33.6 µm x 33.6 µm wide and 60 µm deep object. Empty slices (ES) are added to allow enough space for the extended intensity spread in the WFE simulated image. (b) A simulated CCA image of the object in (a). (c) A simulated SQUBIC WFE intermediate image of the object in (a). Images are shown using different color scales to allow visualization of small intensity values. Lens: 20x/0.8 NA.

4.3 Image restoration from intermediate images

We studied restoration performance of SQUBIC phase mask for both SI and DV EM algorithms First we consider object 1 as described in Section 3.2. The purpose of this simulation is to show the feasibility of using only one PSF to restore beads at different depths. Second we consider another SIEM simulation with only one bead (object 2). This simulation shows the quantitative comparison of depth sensitivity between CCA and SQUBIC imaging system. Lastly, we consider a large object (object 3) to show the performance of WFE imaging system over wide range of depth i.e. up to 60µm. Both SIEM and DVEM restoration results are shown in this case for comparison in order to demonstrate the benefit of using the WFE system.

4.3.1 Restoration in a frame work of space invariant (SIEM) model

SI EM restoration is done to show a comparison study between the restoration performance of CCA and WFE imaging system with SQUBIC phase mask. Three identical beads are considered at an interval of 10 µm (object 1) and the forward simulated image is calculated using the methods described in Section 3.2. The PSF calculated at a 30-µm depth (middle of FOV along z-axis) was used in the SI restoration process. Fig. 3a-c show the xz view of the object and the restored images for both CCA and SQUBIC imaging system. From the restoration results, it can be said qualitatively that, both the location and shape of the middle bead is restored better than the other two beads in case of the CCA imaging system (Fig. 3b) whereas all three beads are restored almost equally in case of the WFE system with SQUBIC phase mask (Fig. 3c). To show a quantitative comparison, we plotted an intensity profile (Fig. 3d) along the diagonal line intersecting each bead as shown in Fig. 3b. The intensity profile is consistent with the qualitative observation and suggests that, we can use the WFE imaging model to minimize computational effort over a 20 µm range without losing significant restoration performance.

To show the decreased depth sensitivity of WFE imaging in terms of a quantitative metric measure, we varied the position of a single bead (object 2) along the z axis from 20 µm to 40 µm and restored a simulated WFE image in each case using a PSF computed at 30 µm. The NMSE between the corresponding objects and restored images for both CCA and WFE SQUBIC imaging system was also computed (based on Eq. 4 but using true and estimated images instead of PSFs) to quantify the restoration results. Fig. 3e shows one of these objects from a set of 11 objects. Fig. 3f shows the NMSE vs. depth of bead (or z-axis position) curve. The WFE imaging system with the SQUBIC phase mask gives approximately 36% NMSE variation whereas the conventional CCA imaging gives almost 73% variation over a 10-µm depth range. Though the NMSE for the CCA imaging system is less than the one obtained for the WFE imaging system when the bead location exactly matches with the PSF location, the rapid variation of the NMSE in the CCA imaging system suggests that, SIEM restoration in the presence of SA leads to restoration artifacts which can only be mitigated using the computationally costly DVEM restoration algorithm for the conventional system. On the other hand, for the SQUBIC WFE system these artifacts are minimized as evident by the slow variation of the NMSE curve (Fig. 3f).

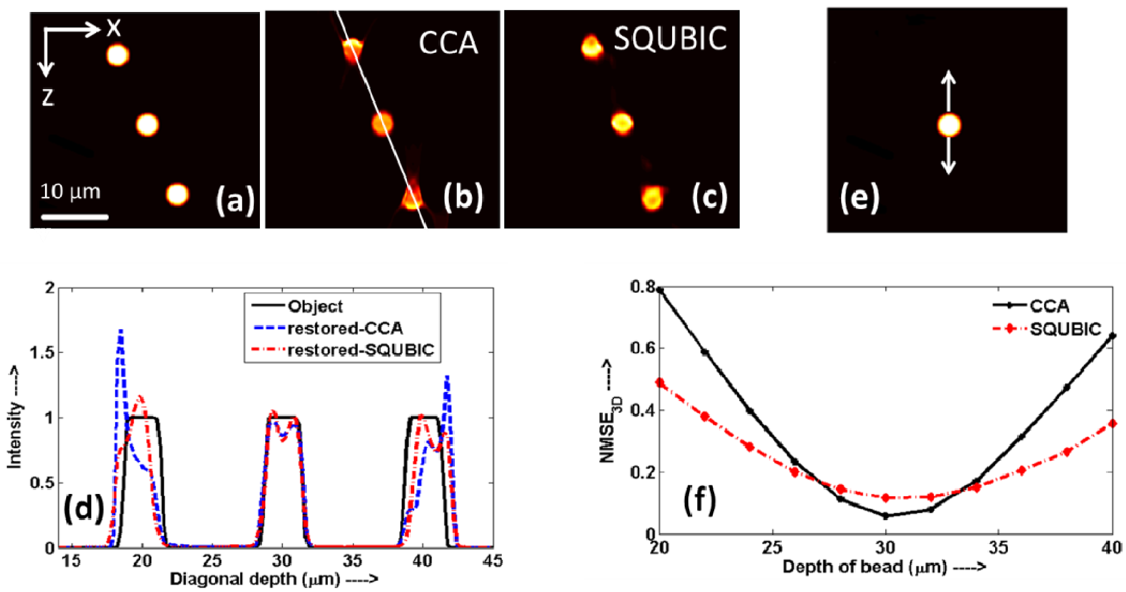

Fig. 3: Performance evaluation of WFE system using the SQUBIC PSF and SI computation. (a) XZ-section image of the object with three beads located at 20 µm, 30 µm and 40µm depth, respectively, below the coverslip. (b) Conventional imaging restoration using the SIEM algorithm and a CCA PSF that is computed at 30 µm depth; (c) similar restoration as in (b) for the modified imaging system using the SQUBIC PSF; (d) intensity profile through the diagonal line shown in figure (b); (e) XZ-section image of an object with a single bead at a 30-µm depth below the coverslip; and (f) $NMSE_{3D}$ restoration analysis of the single bead at a varying depth. The minimum $NMSE_{3D}$ error computed for the SIEM restoration occurs at a 30-µm depth which corresponds to the location of the single PSF. Restored images are displayed at separated nonlinear color scales to show the details in each image. A 20x/0.8 NA air lens is simulated.

4.3.2 Depth variant restoration

To show the comparison study between the restoration performance of CCA and WFE imaging system over a wide range of depth, we simulated the 60 µm deep object with five identical beads as described in section 3.2 (object 3). Fig. 4a-i show the XZ views of the object and the restored images for different kind of restoration techniques including both SIEM and DVEM restoration. Fig. 4b-e are xz views of the restored images for CCA system of which b and c are SIEM restored images with the PSF computed at 0 µm and 30 µm respectively and Fig. 4d-e are restored images with two and five strata DVEM restoration model respectively. Fig. 4f-i are corresponding restored images for the WFE imaging system. From the restoration results it can be said that, for CCA imaging system the SIEM restoration with the 0-µm PSF is the worst whereas for the WFE system significant amount of information can be restored with this PSF. SIEM restored images of WFE imaging system using the PSF computed at 30 µm can sufficiently compete with the five strata DVEM restored images of CCA imaging system which involves five times the computational burden compared to the SIEM restoration.

For a better understanding, we show a quantitative restoration performance by plotting intensity profile along the z axis. This time we did not draw a single line though the center of each bead, rather we took the profile through the line parallel to the z axis. Each time after passing though the center of one bead we shifted along x axis to pass through the center of next bead and hence plotted the intensity vs. depth curve. Fig. 4j shows the intensity vs. depth profile of the

SIEM restoration with the PSF computed at 30 µm. The intensity profile shows that, WFE imaging with SQUBIC phase mask can reasonably reduce the depth sensitivity of the imaging system over a wide range (i.e. up to 60 µm). From the intensity profile of two strata DVEM restoration (Fig. 4k) it can be inferred that, the DVEM restoration technique, is not needed for the WFE imaging system in the case simulated here. This is consistent with the purpose of using the SQUBIC phase mask which is to make the imaging system less sensitive to SA so that SIEM restoration algorithm can sufficiently recover all the necessary information from the blurred microscope images and thereby avoiding the computational burden for the DVEM approach.

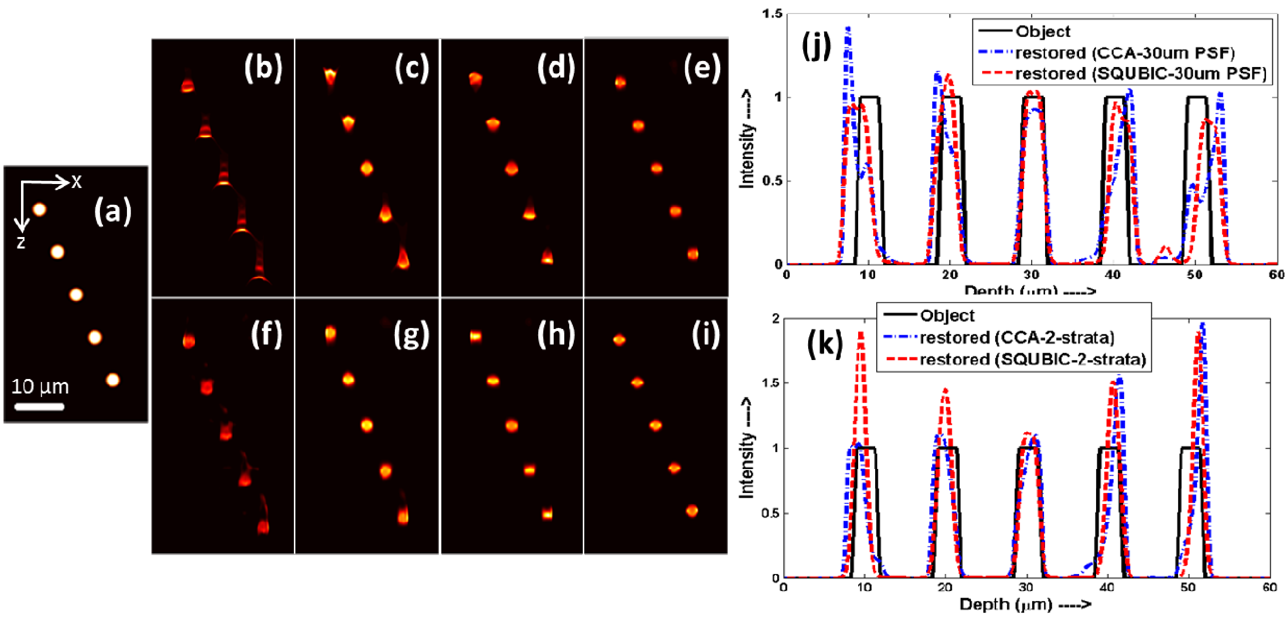

Fig. 4: Performance comparison of WFE systems based on the SQUBIC PSF and either SI or DV restoration. (a) XZ-section image of the object (beads are located axially at 10, 20, 30, 40 and 50 µm); (b) CCA-SIEM restoration using PSF computed at 0 µm, (c) CCA-SIEM restoration using PSF computed at 30 µm; (d) DVEM with two strata restoration (CCA); (e) DVEM with five strata restoration (CCA); (f) SQUBIC-SIEM restoration using PSF computed at 0 µm; (g) SQUBIC-SIEM restoration using PSF computed at 30 µm; (h) DVEM with two strata restoration (SQUBIC); (i) DVEM with five strata restoration (SQUBIC); (j) restoration profile for SIEM (with PSF at 30 µm); (k) restoration profile for two-strata DVEM. Each image is shown to its own scale to show their details. Figure (a)-(i) are drawn to their own scale to show details and figure (j) and (k) are plotted by concatenating lines through the object to get the depth profile. A 20x/0.8 NA air lens is simulated.

5. CONCLUSION

In this paper, we have presented performance of a new WFE imaging approach using a SQUBIC phase mask. Simulation results show that, the effect of depth-induced spherical aberration can be reduced by using a SQUBIC phase mask in the back focal plane of the imaging system. We simulated imaging of 3D sparse beads distributed in a volume over a 60 µm depth and restored these using a single PSF. Simulation results show that the SQUBIC WFE-PSFs are less sensitive to depth-induced SA and beads can be reasonably restored using a space-invariant (SIEM) restoration process whereas, a CCA system requires a DVEM restoration method using a larger number of PSFs resulting in longer computational time. The image restoration process with a SQUBIC WFE-PSFS is therefore faster and requires fewer resources. Wavefront encoding through the SQUBIC phase mask is therefore a solution to decrease depth induced spherical aberration. Through the proper selection of the mask parameter A, its performance can be improved. By using a SLM the SQUBIC phase mask can easily be implemented in an existing microscope setup[16] or alternatively, it can be fabricated lithographically. With the increase of design parameter A, the wrapped phase rapidly changes between $-\pi$ to π and may become difficult to implement the mask practically and fine sampling will be needed in computation which will increase the computational burden[2] . In this study, our concentration was confined to low numerical aperture objective lens. Further study is being performed using a high numerical aperture oil-immersed objective lens.

6. ACKNOWLEDGEMENT

This work is supported by the National Science Foundation (NSF CAREER award DBI-0844682, PI: C. Preza; NSF IDBR award DBI-0852847, PI: C. Preza) and The University of Memphis (through a Herff fellowship to N. Patwary).

7. REFERENCES

[1] G. Saavedra, I. Escobar, R. Martínez-Cuenca *et al.*, “Reduction of spherical-aberration impact in microscopy by wavefront coding,” Optics Express, 17(16), 13810-13818 (2009).

[2] S. Yuan, and C. Preza, “Point-spread function engineering to reduce the impact of spherical aberration on 3D computational fluorescence microscopy imaging,” Optics Express, 19(23), 23298-23314 (2011).

[3] E. R. Dowski, and W. T. Cathey, “Extended depth of field through wave-front coding,” Applied Optics, 34(11), 1859-1866 (1995).

[4] [Computational Imaging Research Laboratory, Computational Optical Sectioning Microscopy Open Source (COSMOS) software package].

[5] C. Preza, and J.-A. Conchello, “Depth-variant maximum-likelihood restoration for three-dimensional fluorescence microscopy,” Journal of the Optical Society of America A-Optics Image Science and Vision, 21, 1593-1601 (2004).

[6] L. S. M. M. Rahman, D. Schuster and C. Preza, "Comparison of computational methods developed to address depth-variant imaging in fluorescence microscopy", SPIE 8589, id. 85890A 7 pp., (2013).

[7] M. J. Booth, M. A. Neil, R. Juškaitis *et al.*, “Adaptive aberration correction in a confocal microscope,” Proceedings of the National Academy of Sciences, 99(9), 5788-5792 (2002).

[8] M. J. Booth, M. Schwertner, T. Wilson *et al.*, “Predictive aberration correction for multilayer optical data storage,” Applied physics letters, 88(3), 031109-031109-3 (2006).

[9] C. Mauclair, A. Mermillod-Blondin, N. Huot *et al.*, “Ultrafast laser writing of homogeneous longitudinal waveguides in glasses using dynamic wavefront correction,” Optics express, 16(8), 5481-5492 (2008).

[10] M. Arigovindan, J. Shaevitz, J. McGowan *et al.*, “A parallel product-convolution approach for representing the depth varying point spread functions in 3D widefield microscopy based on principal component analysis,” Optics express, 18(7), 6461-6476 (2010).

[11] S. Yuan, and C. Preza, "3D fluorescence microscopy imaging accounting for depth-varying point-spread functions predicted by a strata interpolation method and a principal component analysis method." 79040M-79040M-7.

[12] J. W. Goodman, [Introduction to Fourier Optics] McGraw-Hill Book Company, New York(1968).

[13] J. A. Conchello, “Superresolution and convergence properties of the expectation-maximization algorithm for maximum-likelihood deconvolution of incoherent images,” JOSA A, 15(10), 2609-2619 (1998).

[14] S. F. Gibson, and F. Lanni, “Experimental test of an analytical model of aberration in an oil-immersion objective lens used in three-dimensional light microscopy,” Journal of the Optical Society of America A-Optics Image Science and Vision, 9, 54–66 (1992).

[15] O. Haeberlé, “Focusing of light through a stratified medium: a practical approach for computing microscope point spread functions. Part I: Conventional microscopy,” Optics communications, 216(1), 55-63 (2003).

[16] S. V. King, A. Doblas, N. Patwary *et al.*, "Implementation of PSF engineering in high-resolution 3D microscopy imaging with a LCOS (reflective) SLM", “Implementation of PSF Engineering in High-Resolution 3D Microscopy Imaging with a LCoS (Reflective) SLM,” SPIE 8949-39, (2014).